Journal of GeoEngineering, Vol. 14, No. 1, pp. 21-30, March 2019
http://dx.doi.org/10.6310/jog.201903_14(1).3

APPLICABILITY OF COMPLEX WAVELET TRANSFORM TO EVALUATE THE INTEGRITY OF COMMONLY USED PILE TYPES

Sheng-Huoo Ni [1*], Ji-Lung Li [2], Yu-Zhang Yang [2], and Yun-Yui Lai [2]

ABSTRACT

Non-destructive testing techniques are applied to evaluate the integrity of piles. The sonic echo method is usually used to determine the pile tip and the locations of defects. However, the energy of a reflected stress wave is complicated, and it dissipates quickly. It is thus often difficult to evaluate the pile integrity effectively. The purpose of this paper is to utilize the recently developed complex wavelet transform to analyze sonic echo test signals in an attempt to determine the length and location of a defect by analyzing an amplitude spectrogram and phase spectrum in different frequency bands. Several piles of different lengths, materials, cross-sections, and defects were tested to verify the proposed approach. Moreover, the discussion of the wavelet selection, the features of the wave propagation in the pile, and an explanation of the analytical steps are included. The testing results show that a complex wavelet transform can be used to evaluate the integrity of common pile types.

Key words: Non-destructive testing, pile integrity, complex, wavelet transform.

1. INTRODUCTION

Non-destructive testing (NDT) has been used widely to test pile quality, especially in the case of low-strain testing methods, *e.g.*, sonic echo (SE) tests and the impulse response (IR) method (Ni *et al.* 2017), which are used mostly in determining pile length and integrity (Olson 1989). The traditional SE test method provides a way to identify the reflected waves in piles. A time history curve is used to determine the location of impedance change, and the time difference between a direct wave and a reflective wave. Ni *et al.* (Ni *et al.* 2012; Ni *et al.* 2008) performed a series of tests using a continuous wavelet transform (CWT) with piles that were not yet installed in the soil, and the results were significant. Nevertheless, the method failed to detect the reflection signal from defects and the pile tip after the piles were installed into the soil because the reflection signal was weaker. Park and Kim used a harmonic wavelet analysis of wave (HWAW) with the SE method to numerically find the reflection signals of different modes (Hwang and Park 2014; Park and Kim 2006); however, they lacked practical cases to verify the applicability of the method, especially in detecting long piles.

The purpose of this paper is to evaluate the applicability of a complex continuous wavelet transform (CCWT) to determine the pile length, defect locations, and the pile end condition of common pile types using experimental tests. The CCWT utilizes the phase feature, which is able to detect continuity effectively and is unrelated to the magnitude of energy. It is used to decompose a measured signal into several time domain signals with different frequency bands. If the decomposed signals contain phase information, it finds singular signals effectively, and the pile situation can be easily evaluated (Ni *et al.* 2017). In addition, the analysis results of the proposed method compared with the conventional time domain analysis are discussed.

Manuscript received December 1, 2017; revised August 29, 2018; accepted August 29, 2018.
[1*] Professor (corresponding author), Department of Civil Engineering, National Cheng Kung University, Taiwan 70101, R.O.C. (e-mail: tonyni@mail.ncku.edu.tw).
[2] Graduate student, Department of Civil Engineering, National Cheng Kung University, Taiwan 70101, R.O.C.

2. METHODOLOGY

2.1 Sonic Echo Test Method

The sonic echo method is one type of low-strain pile integrity testing methods. Since no great preparation or excessively expensive testing equipment is required, it has been widely adopted. The schematic drawing of this test is shown in Fig. 1. It is an impact hammer testing technique. The resulting time trace is typically made up of transient pulses and reflected responses from the pile. The stress waves, incident wave, and reflected wave are measured as a function of time.

The impulse wave travels from the pile head to the pile tip and then reflects back to the pile head along the direction of the pile length. In a case of known velocity, based on the one-dimensional wave propagation theory, the pile length or the depth of a defect (L) can be calculated as follows:

$$L = \frac{1}{2} \times c \times \Delta t \tag{1}$$

where Δt is the double travel time from the top to the bottom or interface, and c is the stress wave velocity.

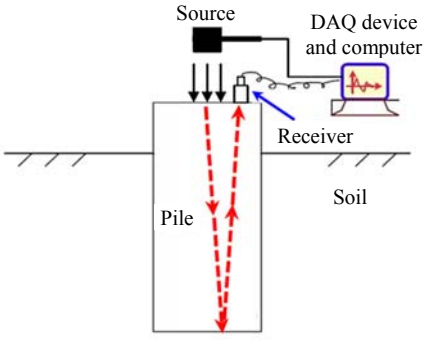

Fig. 1 Schematic drawing of a sonic echo test

In a typical pile foundation, the reflected energy and phase change is due to discontinuous mechanical impedance. The mechanical impedance (Z) of piles is expressed as follows:

$$Z = EA / c = A\sqrt{E\rho} = \rho cA \quad (2)$$

where A is a cross-sectional area; E is Young's modulus; ρ is the density of the pile material. If there are any irregularities in the pile, such as changes in cross-sectional areas or the presence of defects or the pile tip, this will change the mechanical impedance value. Furthermore, when waves propagate through different geometry or the interface of materials, the mechanical impedance ratio (α) can be used to indicate the change as:

$$\alpha = Z_2 / Z_1 \quad (3)$$

This equation means when waves propagate from material Z_1 to Z_2, if α is less than 1, the incident wave and reflected wave are in phase. Conversely, if α is greater than 1, the incident wave and reflected wave are anti-phase. This characteristic can assist engineers with judging variations in the pile and the pile tip position.

2.2 Wave Propagation in the Pile

The stress wave is propagated by the changes in the stress and strain state. The behavior is complex when waves propagate in a bounded elastomer such as piles and slabs (Miklowitz 1978) The reason for this is that there are some reflected waves from the boundary generate mode conversion. After the pressure wave reflects, the shear wave is also generated. In addition, the multiple reflection waves from the boundary add to the complexity of the reflected wave.

The vibrating velocity signal, which can be measured using the SE method, consists of four major components: a direct wave, a reflected P-wave, modal vibration, and noise. Each type of vibrating wave has its own characteristics, which are described as follows:

1. Direct wave: When the pile head surface is impacted, the direct wave arrives at the receiver the fastest. Its energy is very strong, and it has a broadband frequency.
2. Reflected P-wave: As the stress wave is generated on the pile head surface, the energy transfer occurs along the longitudinal direction of the pile. The reflected wave is primarily a pressure wave (P-wave), which vibrates back and forth between the surface of the pile head and the location of the discontinuity. The energy does not decay quickly, and it appears to be progressively longer. If there is no energy decay, the amplitude of the reflected wave will appear periodically.
3. Modal vibration: The modal vibration usually decays very slowly. When the pile head is impacted, the pile mainly generates a longitudinal vibration. Furthermore, the pile is usually affected by the eccentric impulse load, which is accompanied by both lateral vibrations and bending vibrations that affect the velocity spectrum and mechanical admittance curve.
4. Noise: The energy of noise is the weakest and is a natural random vibration. It distributes throughout the entire time domain. The noise is not the signal expected to be retrieved.

Because the tested object is a pile foundation using the SE test method, the wave propagation mode can be simplified as a one-dimensional condition. Therefore, only the reflected P-wave is useful and of concern, and other waves merely complicate the signal. Changes in the energy and phase depend on the different interface conditions along the pile length, so the reflected signal data is collected to analyze the pile integrity and pile tip condition.

The magnitude of a reflected P-wave depends on its damping and dispersive characteristics. However, the phase is only affected by the difference in mechanical impedance. The phase types that correspond to specific pile conditions are as follows: (1) In phase: This phenomenon occurs at the free end of the pile tip when there is a reduction in the cross-section, a weak layer, or a defect in the pile. When the impedance ratio (α) between the materials is less than 1, the incident and reflected waves are in phase, and the phase difference between the incident and reflected wave is 0; (2) Anti-phase: The anti-phase phenomenon occurs at the fixed end of the pile tip, the expansion of a cross-section, or in a hard layer in the pile. When the impedance ratio (α) between the materials is greater than 1, the incident and reflected waves are anti-phase, and the phase difference is 180 degrees (or π).

2.3 Wavelet Transform

The Fourier transform theory is based on breaking a signal down into constituent sinusoids of different frequencies. However, a Fourier analysis has a major drawback, where the time domain information is lost as it transforms the signal from time domain to frequency domain (Ovanesova and Suarez 2004). For practical evaluation of non-stationary physical signals, the results of a Fourier transform lack local information. It cannot provide changes in a specified frequency component with time or signal trends over time.

In order to improve this deficiency, Gabor (1946) adopted a technique called windowing (or the short time Fourier transform, STFT), which maps a signal into a two-dimensional function of time and frequency. The STFT represents a sort of compromise between the time- and frequency-based views of a signal. It provides some information about both when and at what frequencies a signal event occurs. However, it can only offer this information with limited precision, as determined by the size of the window. The drawbacks of the STFT are that only one particular size of time window can be chosen at once, which will apply to all frequencies. Once the window function is chosen, the time and frequency resolution cannot be changed. However, many signals require a more flexible approach, where one can vary the window size to determine a more accurate time or frequency.

Wavelets do this by having a variable window width, which is related to the scale of observation; this flexibility allows the isolation of high-frequency features. One major advantage provided by a wavelet transform (WT) is the ability to perform a local analysis. Therefore, the local features can be described better with wavelets that are concentrated on a localized region.

The major difference is that the STFT has constant time and frequency resolution in contrast to the WT. Another important distinction between a wavelet and a Fourier analysis is that a wavelet analysis is not limited to only sinusoidal functions, but also can be applied to a large selection of localized waveforms as long as they satisfy the predefined mathematical criteria described below.

The WT method has been found particularly useful when analyzing periodic, noisy, intermittent, and transient signals. Considering a complex-value continuous-time function $\psi(t)$, the function integrates to zero, and its square integral, or, equivalent, has finite energy. The function $\psi(t)$ is called a complex-value mother wavelet or a wavelet (Daubechies 1992; Grossmann and Morlet 1984). Let $f(t)$ be any square integrable function. The CWT with respect to a wavelet $\psi(t)$ is defined as

$$W(a,b)=\int_{-\infty}^{+\infty} f(t)\psi_{a,b}(t)dt \tag{4}$$

The $\psi_{a,b}(t)$ is set as

$$\psi_{a,b}(t)=\frac{1}{\sqrt{|a|}}\psi^{*}\left(\frac{t-b}{a}\right) \tag{5}$$

where $W(a, b)$ is wavelet coefficient; a and b are real; * denotes the complex conjugate. The variable a determines the amount of time scaling or dilation, and the variable b represents the time shift or translation. Since the CWT is generated using dilates and translates of the signal function $\psi(t)$, the wavelet for the transformation refers to the mother wavelet.

If the mother wavelet in Eq. (4) is a complex wavelet $\psi_{c,ab}(t)$, Eq. (4) can be rewritten as $W(a,b)=\int_{-\infty}^{+\infty} f(t)\,\psi_{c,ab}(t)\,dt$. This is the complex wavelet transform (CCWT). The real part and imaginary part of a complex wavelet are orthogonal. Then, the instantaneous phase angle of $W(a, b)$ is calculated as follows:

$$\phi(a,b)=\tan^{-1}\left(\frac{W_I(a,b)}{W_R(a,b)}\right) \tag{6}$$

where $W_I(a, b)$ and $W_R(a, b)$ are the imaginary part and the real part of $W(a, b)$, respectively.

In contrast to a real wavelet transform, which only obtains the signal amplitude in one space, CCWT provides additional phase message in two orthogonal spaces. Then, the transformation message for the real part, imaginary part, amplitude, and phase are obtained, which is helpful to analyze the signal.

2.4 Analysis Steps

The pile length or defect can be calculated from the time domain using Eq. (1) after the SE testing is performed. However, if the CCWT is used, where the time-frequency domain and phase spectrum at a particular frequency is completely considered, the analytical procedure is different from time domain analysis of the SE method.

One typical numerical signal of an intact pile with a free end can be obtained from an SE test simulation, as shown in Fig. 2(a). The result of the CCWT is used to plot an amplitude spectrogram, as shown in Fig. 2(b). It is more accurate to calculate the results in a two-dimensional manner. The corresponding phase spectrum is plotted in Fig. 2(c). The magnitude of the phase angle is presented in as a color level image. The red color is 180 degrees (π) of phase angle and the blue color is -180 degrees ($-\pi$) of phase angle in the color level image of the phase spectrum. Note that the energy concentration areas correspond to the shifting phase angle line from π to $-\pi$ in the phase spectrum. Then, the phase diagram (the variation in the phase angle with time) at this specific frequency (*i.e.*, 928 Hz) corresponding to the maximum energy can be plotted, as shown in Fig. 2(d).

When using the SE method with the CCWT to obtain the location of the pile bottom or defects, the procedures are as follows:

Step 1: Find the area of concentrated energy in the amplitude spectrogram, as shown in Fig. 2(b). Then find the phase shift from π to $-\pi$ (or where the phase angle equals 0), which distributes in the form of a straight line from a higher frequency to a lower frequency in the phase spectrum near the corresponding concentrated energy area (see Fig. 2(c)). If the reflected concentrated energy is not obvious, the phase-shift line will be more like a straight line from a higher frequency to a lower frequency. The corresponding time points of the lines (*A-line* and *B-line*) correspond to the incident and reflected wave.

Step 2: Calculate the travel time of wave $\Delta t = t_{B\text{-}line} - t_{A\text{-}line}$ in Fig. 2(c) or Fig. 2(d). The length (or the location of the defect) of the pile can then be calculated using Eq. (1) since the travel time was obtained.

Step 3: Meanwhile, the pile end condition can be determined by the relative phase state of the incident wave and the reflected wave, as shown in Fig. 2(c).

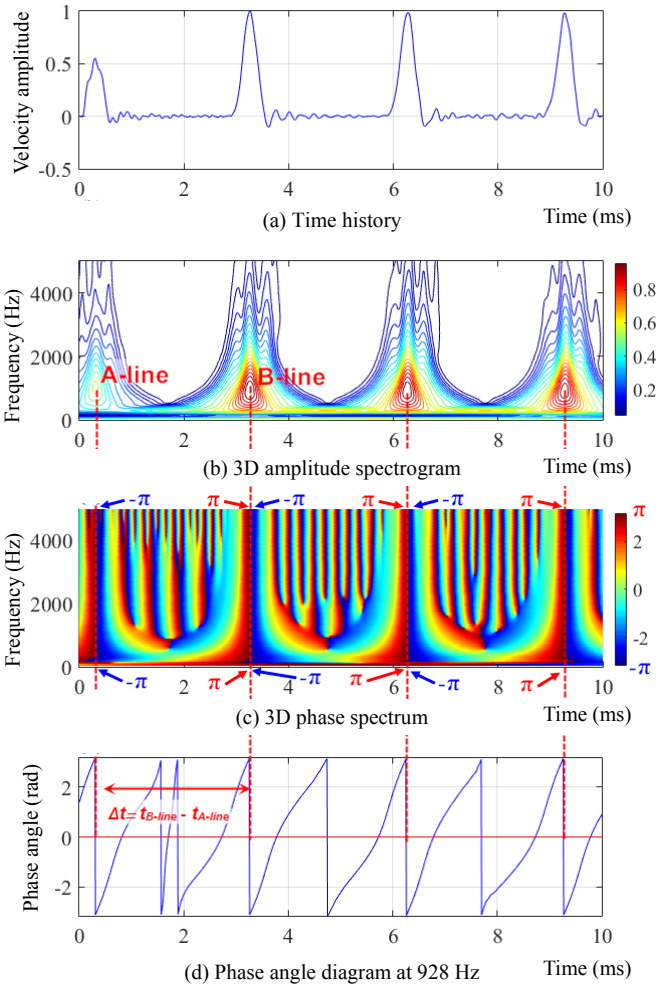

Fig. 2 The analysis results for the simulated intact pile

2.5 Selection of Complex Wavelet

In order to successfully apply the CCWT, it is important to select the most appropriate (or optimal) mother wavelet function to perform the analysis. Complex-valued wavelets provide phase information and are therefore very important in the time-frequency analysis of non-stationary signals. In general, there is an inherent trade-off between the spatial and spectral resolution in the choice of the wavelet. Based on a theory and performance comparison, it is clear that the WT based on a Gaussian function is suitable for signal processing since it can achieve an excellent time and frequency concentration and is able to track the frequency trend at the local time better than other functions (Boultadakis *et al.* 2004). The truncated complex Gaussian function $\psi_G(t)$ is given by the Matlab Wavelet-Toolbox (Misiti *et al.* 2015):

$$\psi_G(t) = C_p\, e^{-t^2} e^{-jt} \tag{7}$$

where the p-th derivative of a complex Gaussian function, denoted by $\psi_G(t)^{(p)}$, can be taken as the mother wavelet. The C_p constant in Eq. (7) is such that the norm of $\psi_G(t)^{(p)}$ is unity.

There are various types of complex Gaussian wavelets. The 1st derivative of a complex Gaussian function (cgau1) and the 2nd derivative of a complex Gaussian function (cgau2) are taken as examples. Their real part, imaginary part, modulus, and phase angle are displayed in Fig. 3. The shape of an incident and reflection wave is like a half sine wave in the SE test. The modulus waveform of cgau2 is more similar to a half sine wave than cgau1, and cgau1 has two spikes that are different from the pile signal. As for the imaginary part, the shape of cgau1 looks similar to that of cgau2. By applying the above complex Gaussian wavelet to the numerical signals discussed in the previous section, the analytical results can be illustrated as shown in Figs. 4 and 5. The amplitude spectrogram obtained from cgau1 shows that there are two energy concentration areas at the location of the incident and reflected wave from the pile bottom. This is different from

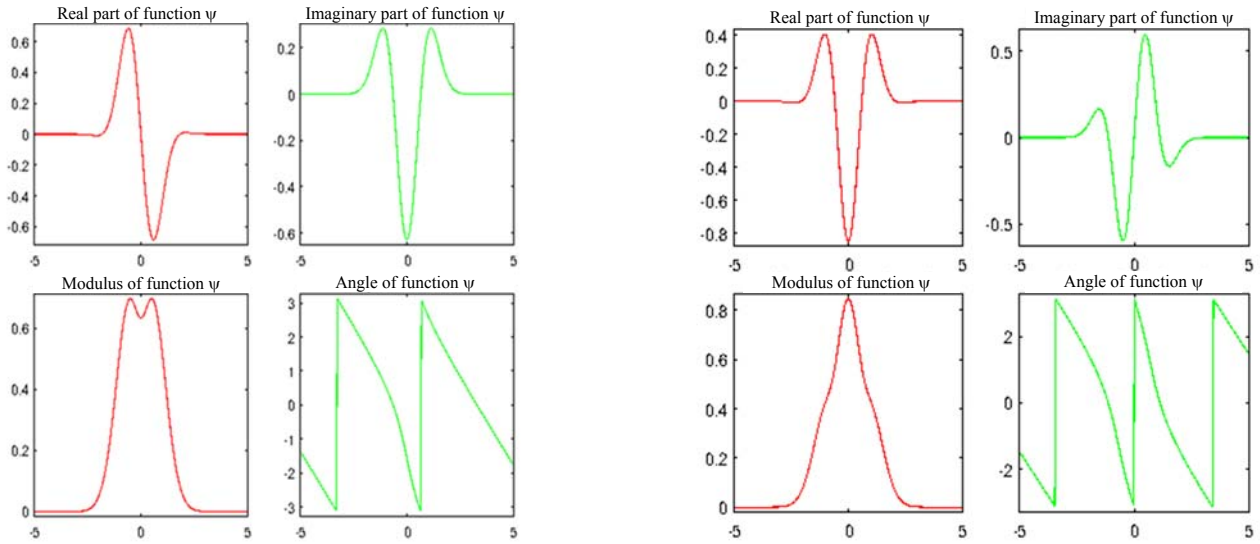

(a) 1st derivative (cgau1) (b) 2nd derivative (cgau2)

Fig. 3 Complex Gaussian function

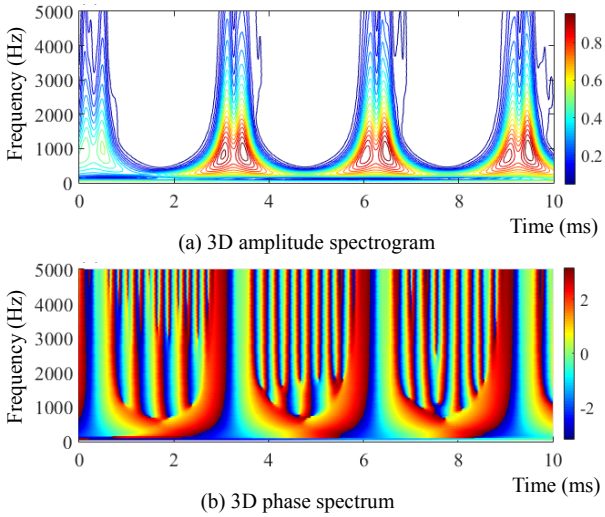

(a) 3D amplitude spectrogram

(b) 3D phase spectrum

Fig. 4 CCWT results of cgau1

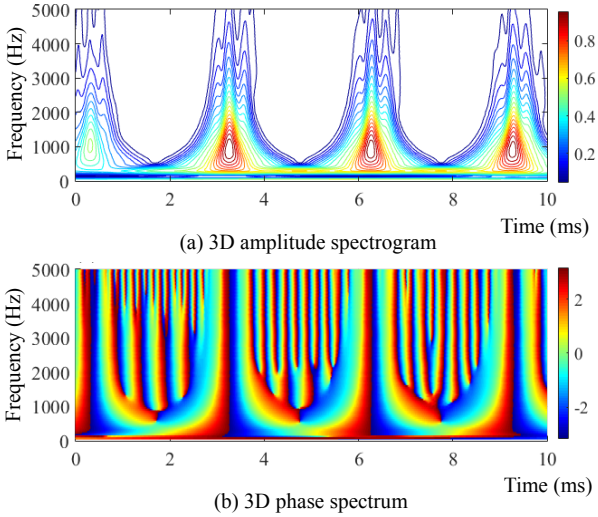

(a) 3D amplitude spectrogram

(b) 3D phase spectrum

Fig. 5 CCWT results of cgau2

the input signal energy characteristic and is clearly not suitable for analyzing the pile signal. On the other hand, when the mother wavelet is cgau2, the analytical result is similar to the feature of the input signal. The similarity of the imaginary part of the mother wavelet indicates that the phase spectra of cgau1 and cgau2 are similar. However, the phase shift from π to −π near the cgau2 energy concentration area is clearer.

According to these screening principles, after comparing the complex Gaussian family, the wavelet transform of cgau2 provides the optimal results for pile signals. Hence, it is adopted for the following analysis.

3. EXPERIMENTAL TEST

3.1 Testing Setup

Several different types of piles were tested in the model and in-situ tests. They were selected to perform a sonic echo test, and the data were analyzed with the CCWT. The model test site is located at the Department of Civil Engineering at National Cheng-Kung University, Taiwan. The layout of these piles and the soil profile are shown in Fig. 6. Piles #M-A and #M-B are 6 m long precast hollow concrete piles, with an outside diameter of 0.3 m and an inside diameter of 0.18 m. Pile #M-A is intact. Pile #M-B is a defective pile with a 0.1 m wide circular defect located 5.1 m from the pile top, and the defective area comprises 30%. Pile #M-C is an 8 m long steel pile. Piles #S-A ~ #S-D are located at different sites in southern Taiwan. Their layout is shown in Fig. 7. Piles #S-A and #S-B are 26 m and 32 m long precast hollow concrete piles, respectively, with outside diameters of 0.8 m and inside diameters of 0.56 m. Piles #S-C and #S-D are 52 m and 58 m long fully cased drilled piles constructed as a bridge foundation, respectively, with a diameter of 1.5 m. Detailed information about these piles, including defects and the stress wave propagation speed, is provided in Table 1.

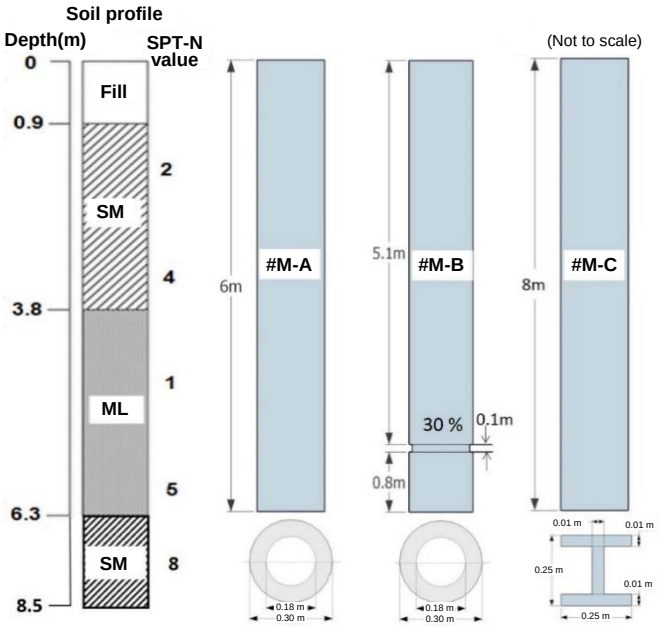

Fig. 6 Layout of model piles and soil profile

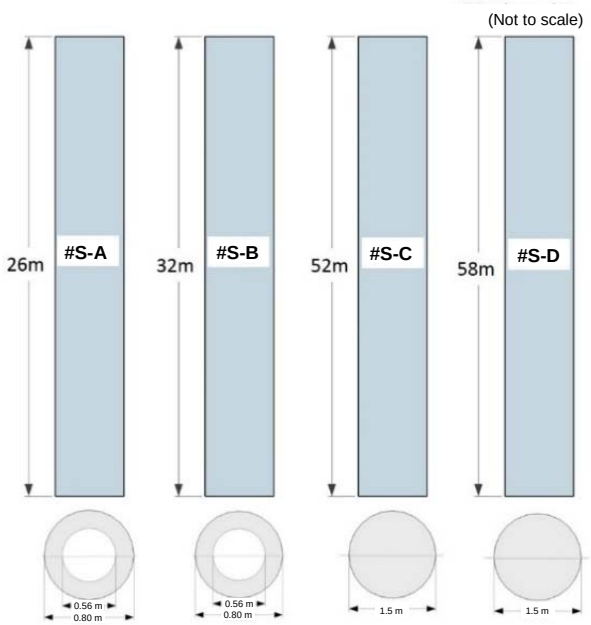

Fig. 7 Layout of in-situ piles

Table 1 Characteristics of the testing piles

Pile label	Pile type	Velocity* (m/s)	Pile length** (m)	Cross-section of pile*** (m)			Type of defect	Depth of defect (m)	Defected area size (%)	Aspect ratio
				D_o	D_i	$H\times B\times t_1\times t_2$				
#M-A	Precast hollow concrete pile	4365	6	0.3	0.18	N/A	intact	N/A	N/A	20
#M-B	Precast hollow concrete pile	4153	6	0.3	0.18	N/A	10cm wide with the circular defect	5.1	30	20
#M-C	Steel Pile	5190	8	N/A		0.25×0.25×0.01×0.01	intact	N/A	N/A	32
#S-A	Precast hollow concrete pile	4084	26	0.8	0.56	N/A	intact	N/A	N/A	33
#S-B	Precast hollow concrete pile	4108	32	0.8	0.56	N/A	intact	N/A	N/A	40
#S-C	drilled pile	4000	52	1.5		N/A	intact	N/A	N/A	35
#S-D	drilled pile	4000	58	1.5		N/A	intact	N/A	N/A	39

* #M-A ~ #M-C and #S-A ~ #S-B: velocity is measured by SE before the piles are embedded in the soil. #S-C ~ #S-D: velocity is assumed.
** #M-A ~ #M-C and #S-A ~ #S-B: pile length is measured before the piles are embedded in the soil. #5 ~ #6: pile length is designed.
*** D_o: Outside diameter; D_i: inside diameter; H: web height; B: Wing width; t_1: web thickness; t_2: wing thickness

3.2 Testing Equipment

In order to obtain high-quality signals from the sonic echo test, the optimal configuration of the force source and data acquisition (DAQ) system is needed. A typical in-situ photo is shown in Fig. 8. The equipment required for an SE test consists of a calibrated impact hammer, a geophone, a DAQ device, and a computer-controlled signal capturer. The details of which are as follows:

1. Force source: The transient force is generated by an impact hammer and applied to the pile surface. There are various impact hammerheads, ranging from soft to hard. Different hammerheads will produce different contact times and input frequencies as well as variations in returning energy. For the field test, a lower frequency and a stronger energy hammer were required. A 5.5 kg (12 lb) hammer was used to generate the pulse source. The hammer was made by PCB Piezotronics, Inc., USA.
2. DAQ system: The components of a DAQ system comprise a sensor, a DAQ device, and a computer. The sensor was a geophone set as a receiver to measure the vibration of the pile. It was a model-L28B receiver produced by Mark Product, U.S.A, which has a natural frequency of 4.5 Hz. The DAQ device and computer were integrated into the model HP35650A analyzer. It is a multi-tasking computer. The DAQ system hardware was combined with the application software for analysis. It was therefore easy to capture signals and process the measurement data. The sampling rate was set up to 124.8 kHz to ensure that high-frequency data would not be missed.

3.3 Analysis of Test Results

3.3.1 Model Tests

Pile #M-A, Pile #M-B, and Pile #M-C were model piles. The time difference between the two phase-shifting lines in the spectrum was calculated. The steps to calculate the pile length or the location of defect were described previously. The analytical results for the different piles were obtained using the CCWT, as shown in Figs. 9 to 11.

Fig. 8 Photo of in-situ site

In the case of Pile #M-A, the energy attenuation with time was observed in the time domain diagram. The incident and reflected signal energy could be found more clearly in the amplitude spectrogram. The traveling time of wave ($\Delta t = t_{B\text{-}line} - t_{A\text{-}line} =$ 2.83 ms) was calculated in the phase spectrum. The time $t_{A\text{-}line}$ and $t_{B\text{-}line}$ corresponded to the locations of the time points along the *A-line* and *B-line*. These two lines were drawn along the energy concentration points in the amplitude spectrogram (see Fig. 9(b)) and the location of the phase shifts from π to −π in the phase spectrum, as shown in Fig. 9(c). Then, the phase diagram (the variations in the phase angle with time at this specific frequency with the energy concentration) (*i.e.*, 960 Hz) could be plotted, as shown in Fig. 9(d).

The depth of the pile tip referenced above could then be calculated with the known stress wave propagation velocity measured before the pile installation. Because the velocity was pre-determined, the pile length was estimated using the proposed procedure. The length of the pile was calculated to be 6.18 m using Eq. (1) (*i.e.*, L = 1/2 × 4365 (m/s) × 2.83 ms). It was close to its true length of 6 m.

It can be seen from Fig. 9(c) that the phase angle of reflected wave corresponding to the maximum energy was at π to −π, which was in phase with the incident wave. Because there was no phase difference between the incident and the reflected wave, the pile end condition of Pile #M-A was a free end boundary condition.

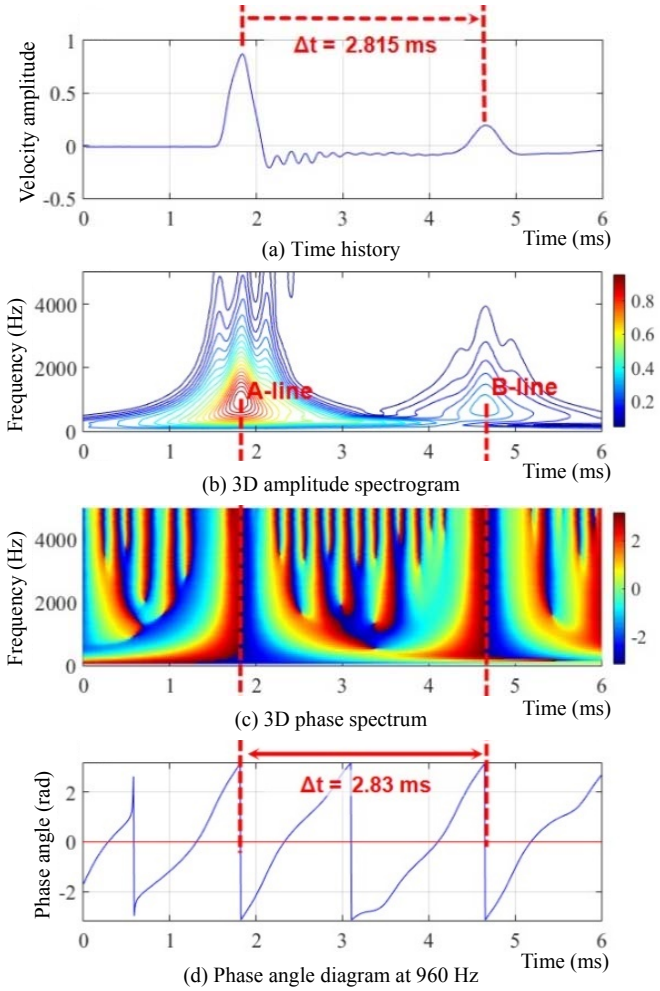

Fig. 9 Analysis results for Pile #M-A

Now considering Pile #M-B, the same procedure could be used to acquire the traveling time of wave (Δt = 2.869 ms), for which the results are shown in Fig. 10, and Eq. (1) is used to calculate pile length, which was found to be 5.96 m (*i.e.*, L = 1/2 × 4153(m/s) × 2.869 ms). The pile tip condition was easy to distinguish, as the energy concentration was located at the phase shift from π to −π, as shown in Fig. 10(c). This verifies this method is useful in finding the pile tip without disturbance, regardless of whether a pile has defects or not. Although Pile #M-B and Pile #M-A were not very different in terms of the amplitude spectrogram pattern, the phase spectrum of Pile #M-B was different from that of Pile #M-A in regard to the defect position. The phase spectrum of Pile #M-A (Fig. 9(c)) showed that there was no phase-shifting line from π to −π in the location of the defect. However, an additional line (*C-line*), the phase-shifting line, was close to the depth of the defect in the phase spectrum of Pile #M-B (see Fig. 10). The phase diagram (the variations in the phase angle with time) at this specific frequency is shown in Fig. 10(e). The depth of the location was calculated to be 4.69 m using Eq. (1). The error was, therefore, less than 10%. This case shows that if the analysis result with CCWT of the intact pile is obtained, it will help to clearly determine the location of defects in the pile.

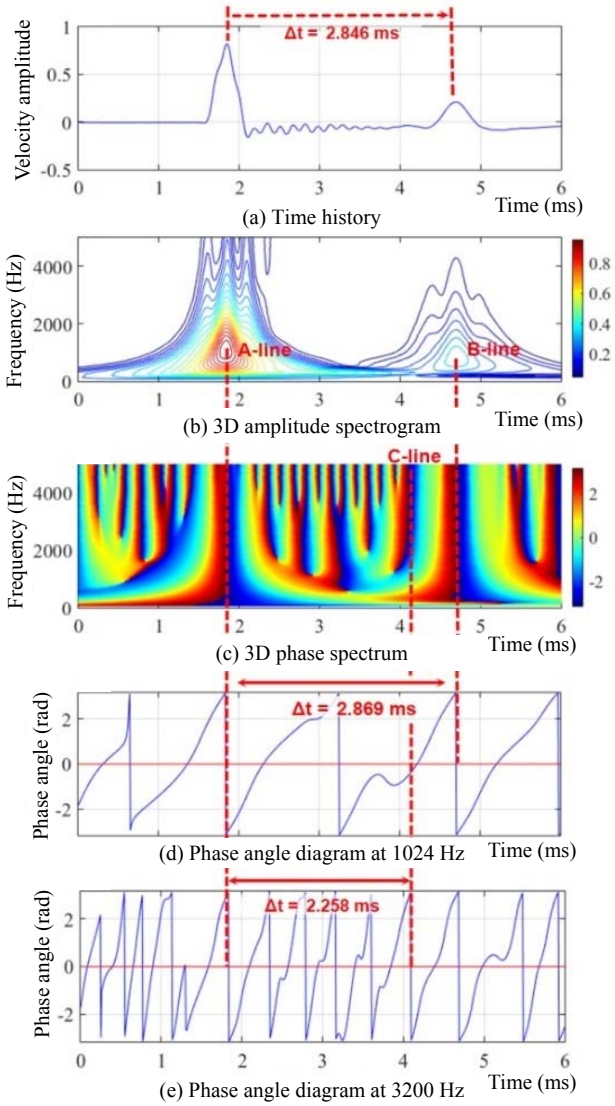

Fig. 10 Analysis results for Pile #M-B

Pile #M-C was an 8 m long steel H-pile. When the impact location and receiver were placed at the junction of the web and the flange on the cross-section of the H-pile surface, an optimal reflected wave signal could be acquired. Because there was enough distance between the impulse and the receiver, the interference of direct waves was less. Moreover, the stress wave energy during propagating in the medium was more concentrated at the junction, and the energy was scattered less. The analytical results are shown in Fig. 11. Through the phase spectrum or the phase angle diagram, the traveling time of the wave was 3.125 ms, and the length of the pile was calculated to be 8.11 m, which was very close to the actual pile length of 8 m. This indicates that this method can be effectively applied to materials other than concrete piles and that the cross-sectional shape is non-circular.

It was determined from these model tests that the amplitude from the wave transform is the magnitude of signal intensity proportional to the square root of the reflected energy. When the testing structure has an interface or boundary, a significant amplitude change can be observed in the amplitude spectrogram. The phase is a continuous measurement of the phase spectrum. The phase change of the stress wave is not affected by the magnitude of the energy. When the wave propagation is in an isotropic and homogeneous medium, it is in a continuous state. In the case of an abnormal condition in the pile, there is a significant change in the phase spectrum, and the variation position can thus be determined.

A higher value of the wavelet coefficient (or amplitude) in a time-frequency domain of a signal is of interest. A variation of the wavelet coefficient indicates that the signal frequency content

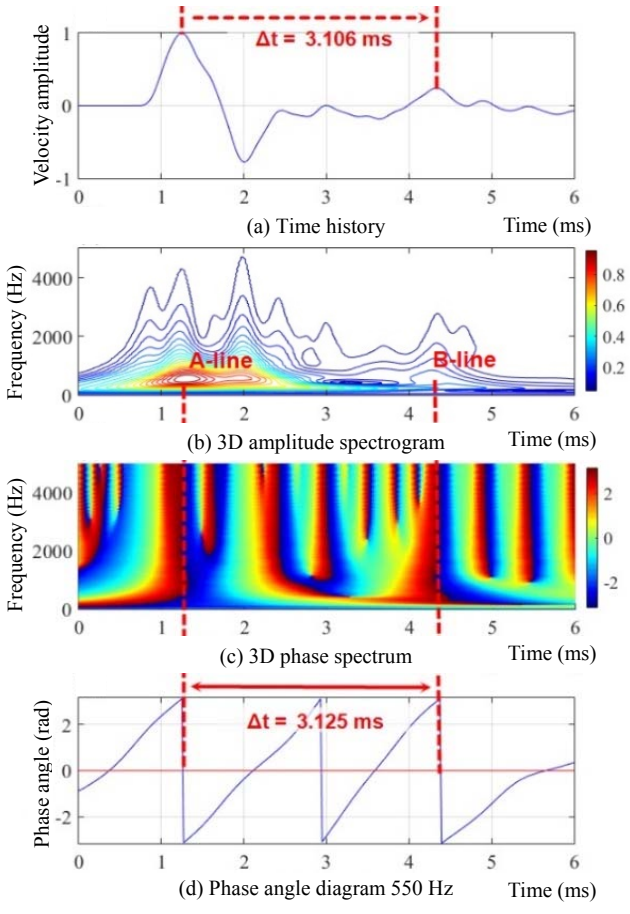

Fig. 11 Analysis results for Pile #M-C

is different. These changes often occur at the interface or boundary. These discontinuities usually cannot be observed from an examination of the structural response in a solely time or frequency domain in piles because of the faint reflected energy. However, they are detectable from the distribution of the amplitude and phase spectrum obtained by the CCWT.

3.3.2 In-Situ Tests

Pile #S-A and Pile #S-B were 26 m and 32 m long precast concrete piles, respectively. The cross-sectional shape was a hollow circle similar to that of Pile #M-A. However, the length and cross-section size were different. The measurement signal analyzed by the CCWT is shown in Figs. 12 and 13. The major differences from the model pile are that the signal energy obtained was weaker and more complicated. The time domain interpretations of end reflection are marked with question marks to indicate that the end reflection point cannot easily identify in the time domain data. Through the method proposed in this paper, the incident of a reflected wave can be determined by the amplitude spectrogram, phase spectrum, or phase angle diagram. The analyzed lengths were as follows: Pile # S-A pile was 27.48 m, with an error of 5.67 %. Pile #S-B was 31.97 m, with an error of –0.09 %. This verifies that the proposed approach is also applicable to concrete hollow piles with different aspect ratios.

In-situ cases of the long, drilled piles (Pile #S-C and Pile #S-D) were performed. Their lengths were designed to be 52 m and 58 m, respectively. The analytical results for these piles were obtained using the CCWT, as shown in Figs. 14 and 15. The echo energy was so weak that it was difficult to use the traditional time-domain analysis method to determine the maximum amplitude of the reflected P-wave. It was also not easy to identify the pile tip energy using only the amplitude spectrogram. In contrast, through the proposed method, the time position of the reflected wave was obtained by the phase spectrum of Pile #S-C. From the phase spectrum, the phase shifted from π to −π through full frequencies near the location of pile bottom, as shown in Fig. 14(c). The phases were in phase in the location of both the pile head and pile tip (*i.e.*, no phase difference). The phase characteristic feature shows that the pile was a free end. The phase diagram at this specific frequency (*i.e.*, 112 Hz) with the energy concentration could be plotted and is shown in Fig. 14. From the phase spectrum of Pile #S-D, it can be seen that the phase at the pile bottom is 0, and the location is the light green area in Fig. 15(c). The phase at pile head and pile tip are anti-phase (*i.e.*, the phase difference is π). The phase characteristic feature shows that the pile is a fixed end. The phase diagram at this specific frequency (*i.e.*, 144 Hz) with the energy concentration location can be plotted as shown in Fig. 15. Meanwhile, the pile length of Pile #S-C and Pile #S-D was calculated using the aforementioned steps. The errors in each pile length test were within 5%. This indicates that the evaluation of pile length is not affected by an increase in the pile length.

The Pile #S-C and Pile #S-D signals were obtained at the construction site. In the absence of the precise wave propagation velocity of the pile, the wave velocity was assumed to be 4000 m/sec. Moreover, the length of the constructed pile may have differed from the designed length, which may have caused errors in the evaluation of the true pile length.

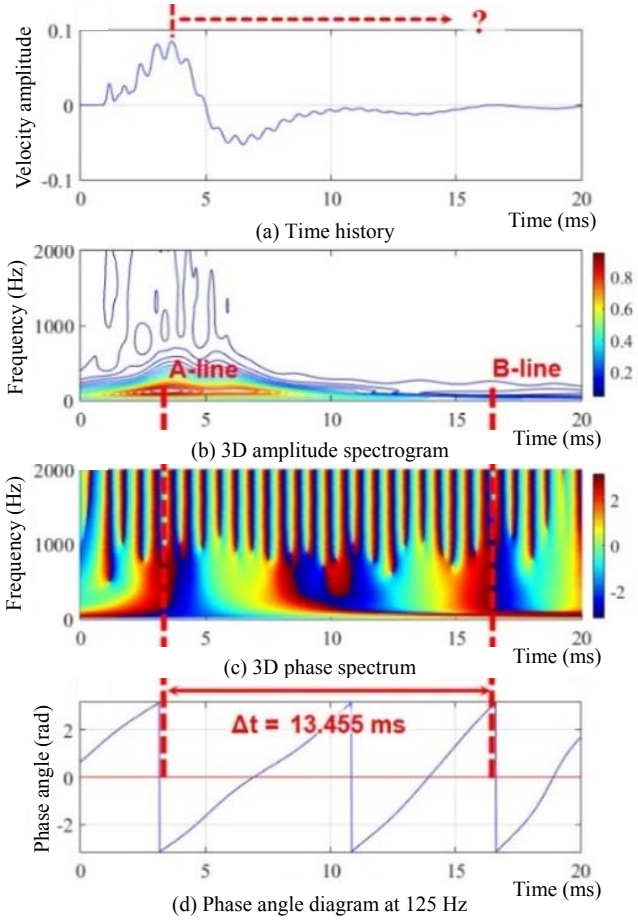

Fig. 12 Analysis results for Pile #S-A

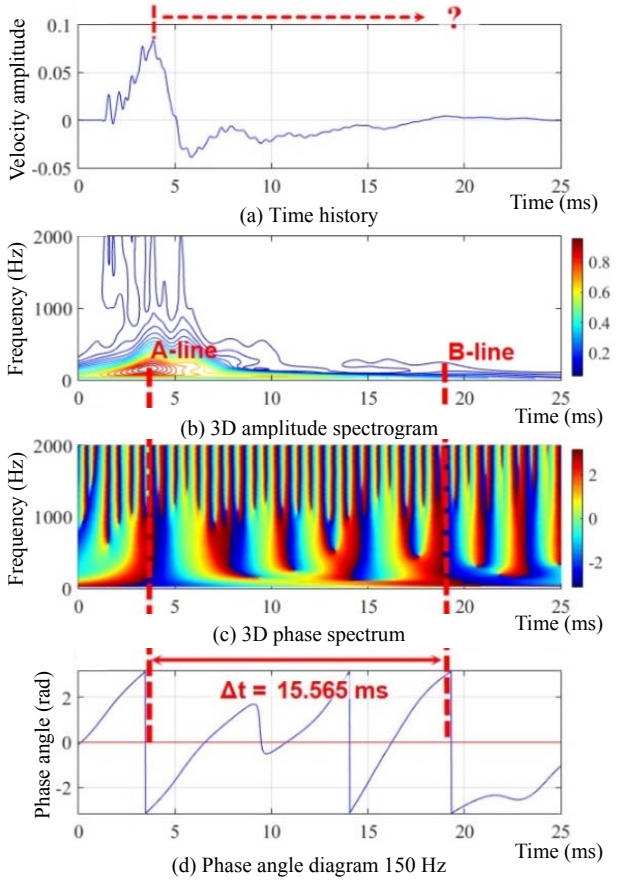

Fig. 13 Analysis results for Pile #S-B

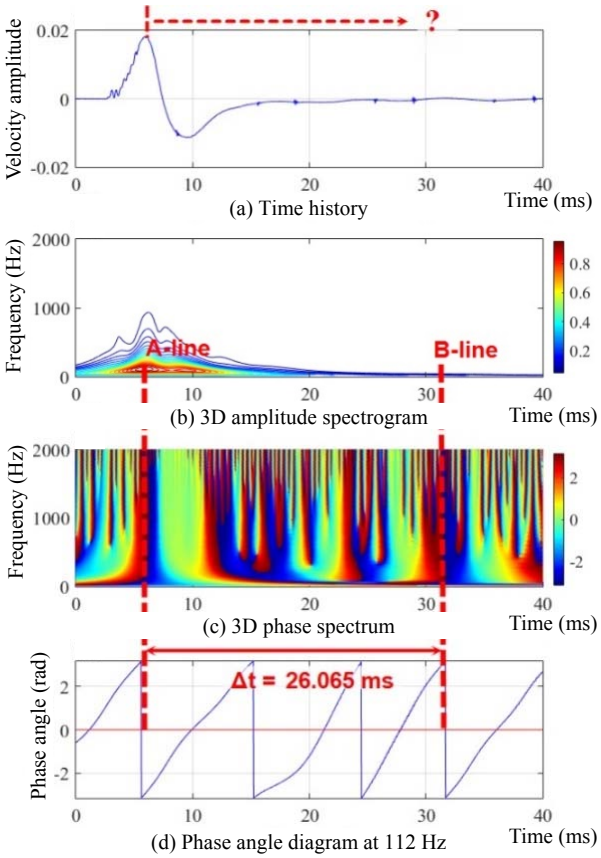

Fig. 14 Analysis results for Pile #S-C

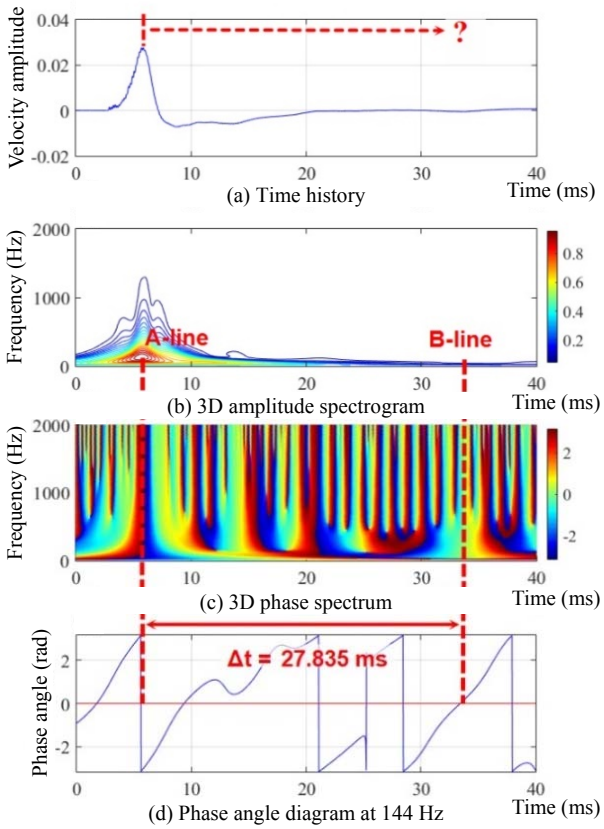

Fig. 15 Analysis results for Pile #S-D

3.4 Discussion of Test Results

The results of each pile evaluation are summarized in Table 2. The errors in the calculated pile lengths were mostly less than 5%, which shows that the proposed method can be used to effectively estimate the pile length. The evaluation results are significantly better than those obtained using the traditional SE method analysis. This indicates that the proposed approach is also applicable for different types of piles, such as piles with defects, different cross-sectional shapes, pile materials, pile lengths, and aspect ratios.

From the above experimental tests, in the case of a defective or long pile, even though only a faint signal is captured, the suggested approach is still able to identify the pile information and effectively determine the position of the discontinuity. These results enhance the applicability of this method. When the pile is defective, the existence and location of the defect can be determined by the difference in the pattern of the phase spectrum. The location of the defect is calculated by the phase shift in the phase spectrum, for which the results are generally acceptable.

When the incident and reflected waves are both located at the phase shift of $\pi \sim -\pi$ (*i.e.,* in phase) in the phase spectrum, this indicates the pile is a friction pile. When the incident wave signal is located at the phase shift of $\pi \sim -\pi$, and the reflected wave signal is at the 0 phase (*i.e.*, anti-phase), this indicates the pile is a bearing pile. These features are easily visible from the phase spectrum and are consistent with real situations.

Table 2 Summary of the test results

Pile label	Pile type	Pile length/defect location*(m)	Estimated pile length/defect location (m)		Error (%)		Pile tip condition
			CCWT	SE	CCWT	SE	
Pile #M-A	Precast hollow concrete pile	6	6.18	6.14	2.94	2.4	Free end
Pile #M-B	Precast hollow concrete pile with the defect	6	5.96	5.91	– 0.71	– 1.5	Free end
	Defect location	5.1	4.69	4.66	– 8.06	– 8.67	
Pile #M-C	Steel pile	8	8.11	8.06	1.37	0.75	Free end
Pile #S-A	Precast hollow concrete pile	26	27.48	27.92	5.67	7.39	Free end
Pile #S-B	Precast hollow concrete pile	32	31.97	31.29	– 0.09	– 2.22	Free end
Pile #S-C	Drilled pile	52	52.13	52.79	0.25	1.52	Free end
Pile #S-D	Drilled pile	58	55.67	55.66	– 4.02	– 4.03	Fixed end

* #M-A ~ #S-B: Pile length/defect location is measured before piles are embedded in the soil. #S-C and #S-D: Pile length is designed.

4. CONCLUSIONS

A suitable wavelet is selected in this work, and an approach using a sonic echo test method with the CCWT is proposed to evaluate the integrity of the pile under consideration. The approach procedure is described in the paper. It takes advantage of the degree of sensitivity by which the phase can respond to the discontinuity of the interface. Utilizing the complex number characteristics of the CCWT can highlight the phase angle information of a reflected signal. Thus, the integrity of a pile can be much easy to be judged. The signals of testing piles successfully verified the suitability and applicability of this approach. The analysis results were close to a real situation and superior to those obtained using the traditional SE time domain method.

The major advantage of this method is that faint or complex reflected pile waves are easy to identify in the phase spectrum. Because the characteristics of both the real and imaginary part of a complex wavelet can be obtained using the CCWT, the available wavelet coefficients (or amplitude) and phase spectrum information can effectively improve the identification of the pile signal singularity and can extract the most useful signal and determine the location of the pile tip and determine the pile end condition.

ACKNOWLEDGEMENTS

This study was supported by the Ministry of Science and Technology under Grant No. MOST 104-2221-E-006-206, Taiwan, R.O.C. The authors would like to express their special thanks to all other participants in this project.

REFERENCES

Boultadakis, G., Skrapas, K., and Frangos, P. (2004). "Time-frequency analysis of radar signals," *RTO-MP-SET-80*, 7-1-7-20.

Daubechies, I. (1992). *Ten Lectures on Wavelets*, Vol. 61, SIAM. https://doi.org/10.1137/1.9781611970104

Gabor, D. (1946). "Theory of communication. Part 1: The analysis of information." *Journal of the Institution of Electrical Engineers - Part III: Radio and Communication Engineering*, **93**(26), 429-441. http://dx.doi.org/10.1049/ji-3-2.1946.0074

Grossmann, A. and Morlet, J. (1984). "Decomposition of Hardy functions into square integrable wavelets of constant shape." *SIAM Journal on Mathematical Analysis*, **15**(4), 723-736. https://doi.org/10.1137/0515056

Hwang, H.J. and Park, H.C. (2014). "Evaluation of condition of gravel ballast layer on high-speed railway using surface wave method based on harmonic wavelet analysis of waves." *NDT & E International*, **68**, 78-87. https://doi.org/10.1016/j.ndteint.2014.08.005

Miklowitz, J. (1978). *The Theory of Elastic Waves and Waveguides*. North-Holland Publishing Company.

Misiti, M., Misiti, Y., Oppenheim, G., and Poggi, J.M. (2015). *Wavelet Toolbox: For Use with MATLAB*.

Ni, S.H., Isenhower, W.M., and Huang, Y.H. (2012). "Continuous wavelet transform technique for low-strain integrity testing of deep drilled shafts." *Journal of GeoEngineering*, TGS, **7**(3), 097-105. https://doi.org/10.6310/jog.2012.7(3).3

Ni, S.H., Li, J.L., Yang, Y.Z., and Yang, Z.T. (2017). "An improved approach to evaluating pile length using complex continuous wavelet transform analysis." *Insight - Non-Destructive Testing and Condition Monitoring (The Journal of the British Institute of Non-Destructive Testing)*, **59**(6), 1-7. https://doi.org/10.1784/insi.2017.59.6.318

Ni, S.H., Lo, K.F., Lehmann, L., and Huang, Y.H. (2008). "Time-frequency analyses of pile-integrity testing using wavelet transform." *Computers and Geotechnics*, **35**(4), 600-607. https://doi.org/10.1016/j.compgeo.2007.09.003

Ni, S.H., Yang, Y.Z., and Lyu, C.R. (2017). "Application of wavelet analysis for the impulse response of pile," *Smart Structures and Systems*, **19**(5), 513-521. https://doi.org/10.12989/sss.2017.19.5.513

Park, H.C. and Kim, D.S. (2006). "Non-destructive pile integrity test using HWAW method." *Key Engineering Materials*, **321**, 363-366. https://doi.org/10.4028/0-87849-412-x.363